Enhanced Electrocatalytic Oxygen Evolution in Au–Fe Nanoalloys

*Irene Vassalini, Laura Borgese, Michele Mariz, Stefano Polizzi, Giuliana Aquilanti,
Paolo Ghigna, Andrea Sartorel, Vincenzo Amendola,* and Ivano Alessandri**

Abstract: *Oxygen evolution reaction (OER) is the most critical
step in water splitting, still limiting the development of efficient
alkaline water electrolyzers. Here we investigate the OER
activity of Au–Fe nanoalloys obtained by laser-ablation syn-
thesis in solution. This method allows a high amount of iron
(up to 11 at %) to be incorporated into the gold lattice, which is
not possible in Au–Fe alloys synthesized by other routes, due to
thermodynamic constraints. The $Au_{0.89}Fe_{0.11}$ nanoalloys exhibit
strongly enhanced OER in comparison to the individual pure
metal nanoparticles, lowering the onset of OER and increasing
up to 20 times the current density in alkaline aqueous solutions.
Such a remarkable electrocatalytic activity is associated to
nanoalloying, as demonstrated by comparative examples with
physical mixtures of gold and iron nanoparticles. These results
open attractive scenarios to the use of kinetically stable
nanoalloys for catalysis and energy conversion.*

The intrinsic slow kinetics of oxygen evolution reaction
(OER) represents a major obstacle towards the development
of efficient electrochemical or photoelectrochemical cells for
water splitting.[1] In alkaline media, OER occurs through the
consumption of hydroxy ions to produce oxygen and water
$(4\,OH^- \rightleftarrows O_2 + 2\,H_2O + 4\,e^-)$. Various combinations of metals,
oxides, mixed-metals and alloys have been investigated as
catalysts to improve OER kinetics.[2] In particular, mixed-
metal or alloy electrodes are attracting great interest as viable
alternatives to the expensive Ru and Ir-based catalysts.[3–5] In
this context, iron is gaining ever-increasing interest as an

OER active component, either alone or in combination with
other metals.[6,7] Various research groups demonstrated that
Fe^{3+} plays a key role in OER.[8–15] This fact was not clearly
realized before, because the observation of a significant
improvement of OER activity was hampered by the poor
conductivity of the OER-active material containing the Fe^{3+}
species, typically FeOOH.[14] On the other hand, lower values
of overpotential and remarkable catalytic efficiency were
observed in the case of Fe^{3+} species combined with more
conductive host materials, like CoOOH or NiOOH.[11–15] Two
recent papers reported a significant improvement of OER
activity in alkaline conditions when the surface of gold was
doped with Fe^{3+} species.[14,15] However, these electrodes are
formed upon alkaline oxidation of Au surfaces and subse-
quent adsorption of Fe^{3+} OER active sites, which does not
allow a precise control of iron-loading and overall chemical
composition. The formation of Au–Fe nanoalloys could
provide an interesting alternative for obtaining high surface
area Au–Fe OER-active materials with a controlled compo-
sition and, in general, new catalysts for different types of
reactions, as suggested by Martirez and Carter.[16] The main
issue related to Au–Fe alloys is the low miscibility of the two
metals. Their thermodynamic stability in ambient conditions
is indeed restricted to a low Fe content (< 2.5 at %),[17] which
does not allow for a significant enhancement of the OER
activity.

Here we report the first experimental observation of the
enhancement of OER in Au–Fe nanoalloys achieved by laser-
ablation synthesis in solution (LASiS), which enables the
production of kinetically stable and homogeneous nanoalloys
with content of Fe well above the thermodynamic limit (up to
11 at %), thanks to the fast kinetics of nanoparticles formation
(Figure 1a and Figure S1 in the Supporting Information).

Importantly, LASiS is a "one-step", easily scalable
process, which starts from an already formed kinetically
stable Au–Fe bulk alloy target.[18] The obtained nanoalloys
retain the face centred cubic (fcc) structure of Au, though
with Fe atoms as substitutional dopants (Figure 1b–d).
XANES (X-ray absorption near edge structure) spectra
collected at the Fe-K and Au-L_{III} edges (Figure 1e,f, respec-
tively), and the corresponding derivatives (Figures 1g,h),
show that iron electronic structure is heavily modified in the
nanoalloy, while the gold fingerprint remains very similar to
that of the pure metal. At Fe K-edge the onset of absorption is
at 7112 eV corresponding to that of metallic iron (Figure 1g
and inset of Figure 1e). This evidences a significant contri-
bution of metal Fe states near the Fermi level, as typically
observed for the alloys of noble metals with fcc structure with
iron.[38]

The formation of an intermetallic alloy is further con-
firmed by the EXAFS (extended X-ray absorption fine

[*] Dr. I. Vassalini, Dr. L. Borgese, Prof. I. Alessandri
INSTM and University of Brescia, Mechanical and Industrial
Engineering Department (DIMI)
via Branze 38, 25123 Brescia (Italy)
E-mail: ivano.alessandri@unibs.it

M. Mariz, Prof. A. Sartorel, Prof. V. Amendola
INSTM and Department of Chemical Sciences, University of Padova
via Marzolo 1, 35131 Padova (Italy)
E-mail: vincenzo.amendola@unipd.it

Prof. S. Polizzi
Department of Molecular Sciences and Nanosystems, Centro di
Microscopia Elettronica G. Stevanato, Università Ca' Foscari Venezia
and INSTM UdR Venezia
30172 Venezia-Mestre (Italy)

Dr. G. Aquilanti
Elettra-Sincrotrone Trieste
s.s. 14, km 163.5, 34149 Basovizza, Trieste (Italy)

Prof. P. Ghigna
INSTM and Department of Chemistry, University of Pavia
viale Taramelli 13, 27100 Pavia (Italy)

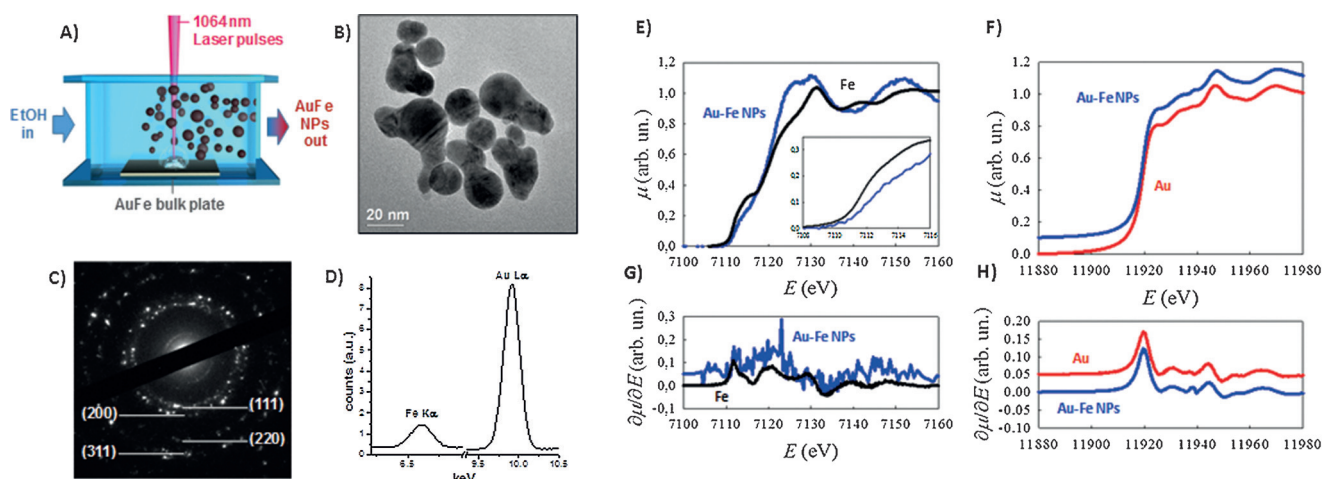**Figure 1.** A) Sketch of LASiS of Au–Fe NPs. B–D) Transmission electron microscopy analysis of $Au_{0.89}Fe_{0.11}$ nanoalloys: B) representative bright field image of alloy NPs; C) selected area electron diffraction pattern, showing typical reflection of the face-centred cubic cell of these alloys; D) energy dispersive X-ray spectroscopy analysis showing the coexistence of Fe (Kα peak) and Au (Lα peak) in the nanoalloy. E–H) XANES spectra at the Fe-K edge (blue line in (E)) and at the Au-L_{III} edge (blue line in (F)) of the $Au_{0.89}Fe_{0.11}$ nanoalloys, and the corresponding derivatives (blue lines in (G) and (H) for Fe and Au edges, respectively). The spectra of pure metal Fe (black lines) and Au (red lines) are also shown for comparison. The inset in panel (E) shows an enlarged view of the low-energy region of the Fe-K edge.

structure) at the Au-L_{III} edge, showing a slight decrease in the Au-nearest neighbor distance with respect to the Au–Au distance in pure bulk gold (Figure S1.2).

Information on the local electronic structure of Fe can be obtained by looking at the inset in Figure 1e, where the low energy part of the Fe K-edge spectrum is shown on an enlarged energy scale. This region is dominated by electronic transition to empty energy levels. In particular, the weak structures slightly above 7110 eV are due to transitions from the Fe 1s level to hybridized s,d bands, while the large shoulder in the absorption between 7111 and 7116 eV is due to transitions to p-like states above the Fermi level.[39] Comparison between the spectrum of the Au–Fe nanoalloy and that of metallic Fe shows a marked decrease in the spectral weight for the transition to the p-like states for the alloy, while the transition to the s,d bands seems to be unaltered. Thus, a strong hybridization with Au states is deduced, lowering the density of the p-like states as projected on Fe, reasonably due to large delocalisation effects.

Another key aspect of laser-generated nanoparticles is that they are not protected by any organic or undesired capping agent, which explains their excellent performances in recently reported catalytic applications.[19–22] X-ray photoelectron analysis (Figure S1.3) shows that the surface of Au–Fe nanoalloys obtained from LASiS is composed only of metal Au and oxidized Fe, constituting a passivation layer that confers to the nanoalloy excellent stability in air and water environment.[18] The surface of the Au–Fe nanoalloys is accessible for reactants and their catalytic activity can be investigated without any limitations or spurious effects owing to the protecting species. Taking advantage of the above-mentioned peculiarities, in this work we investigated the electrochemical reactivity in alkaline aqueous environment (1M KOH) of Au–Fe alloy nanoparticles (NPs) with atomic composition Au 89 at% and Fe 11 at%, and compared their performances with other Au–Fe alloy NPs containing a lower

amount of iron (8 at% and 3 at%), as well as with pure gold NPs, iron oxide (FeO$_x$) NPs and a physical mixture of Au and FeO$_x$ NPs, all of them obtained by the same LASiS protocol.

The electrocatalytic activity of the NPs was investigated by means of cyclic voltammetry (CV) and electrochemical impedance spectroscopy (EIS). The experimental details on NP fabrication and the electrochemical experiments are reported in the Supporting Information (Chapters S1 and S2).

The CV of all samples supported on indium tin oxide (ITO) coated glass electrodes and tested in 1M KOH are shown in Figure 2a. The $Au_{0.89}Fe_{0.11}$ NPs exhibit a remarkable improvement of OER activity in comparison to the Au and FeO$_x$ NPs. The decrease of the iron content from 11 to 8 at% does not produce any relevant changes in the OER activity, while the behavior of $Au_{0.97}Fe_{0.03}$ is more similar to that of pure Au NPs. Figure 2b shows a comparison of the relative values of overpotential (η) required to achieve a current density of 10 mA cm^{-2}, which is considered a relevant figure of merit in view of practical applications based on solar-to-fuel conversion.[40] In particular, the results reveal that AuFe NPs with the highest iron content (8 and 11 at%) reach 10 mA cm^{-2} at $\eta \approx 0.8$ V. Although still far from IrO$_2$ and RuO$_2$ ($\eta_{J=10\,\mathrm{mA\,cm}^{-2}} = 0.43$),[41] which are the most efficient electrocatalysts for OER, this value is about 0.4 V lower than that obtained with FeO$_x$ NPs (1.17 V) and even 1 V lower than that of pure Au NPs (1.8 V). This demonstrates that AuFe NP alloys incorporating an iron content well above the thermodynamic limit (8–11%) offer a new route for enhancing the OER efficiency.

Figure 2c shows that the onset of OER is also significantly shifted to lower potential values for both $Au_{0.89}Fe_{0.11}$ and $Au_{0.92}Fe_{0.08}$ ($\Delta E_{onset} \approx 0.1$ V in comparison to the other counterparts). 1.82 V vs. RHE has been chosen as reference potential for the following evaluations of current density, EIS measurements and accelerated stability tests, because at this potential value all the considered systems are under OER
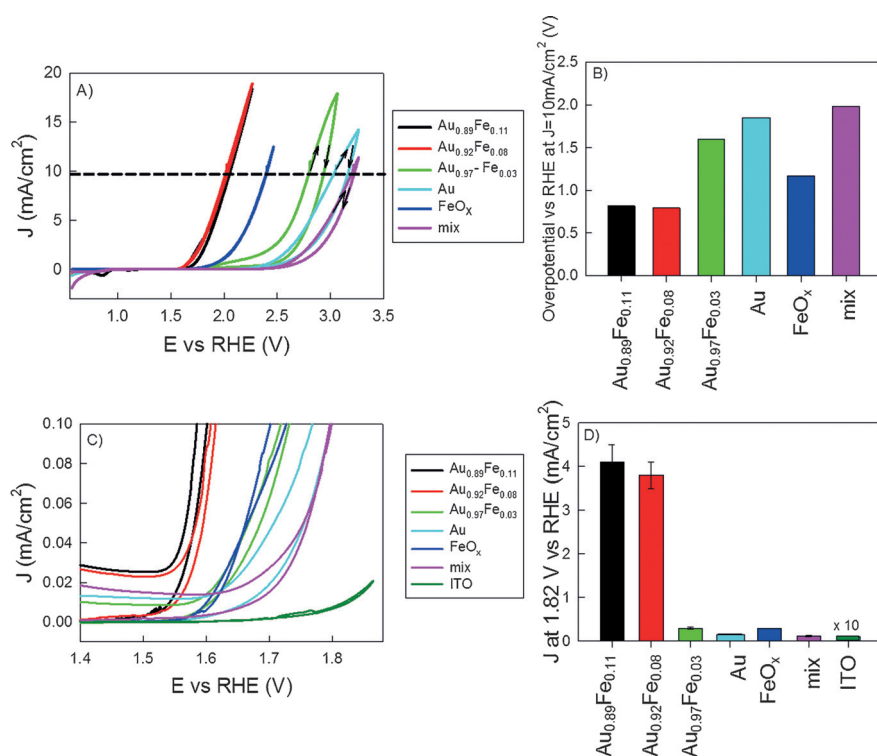
Figure 2. Comparison of cyclic voltammetry performed with different Au–Fe nanoalloys, Au, FeO$_x$ and mixed Au/FeO$_x$ NPs supported on ITO coated glass in 1 M KOH. A) Cyclic voltammetry (CV) extended from 0 to 3.3 V vs. RHE, in order to obtain a current density $J = 10$ mA cm^{-2} for all the samples under analysis. B) Comparison of the overpotential required to achieve a current density $J = 10$ mA cm^{-2} extrapolated from the CV experiments reported in panel (A) for the different NPs. C) Zoom of the CV data in the potential range 1.4–1.87 V vs. RHE. The CV of naked ITO electrode is reported as a reference. D) Current density at 1.82 V vs. RHE. Data extrapolated from CV acquired from three independently prepared electrodes.

conditions. Figure 2d shows that at 1.82 V the current density value of the alloy Au$_{0.89}$Fe$_{0.11}$ is ca. 4 mA cm^{-2}, about 23, 13 and 30 times higher than that of Au, FeO$_x$ and the physical mixture of Au and FeO$_x$ NPs, respectively. The turnover

frequency (TOF), calculated according to Jaramillo and co-workers,[29] was 0.09 s^{-1} at 1.82 V. The current density reaches its maximum (18.8 mA cm^{-2}) at $E = 2.3$ V vs. RHE, with a Faradaic yield > 95 % (see Chapter S2).[25]

A further confirmation of the improved oxygen evolution activity of Au–Fe nanoalloys resulted from electrochemical impedance spectroscopy analysis. Figure 3 shows Nyquist plots of Au$_{0.89}$Fe$_{0.11}$, Au, FeO$_x$ and the mixture of Au/FeO$_x$ NPs, upon acquisition between 1 Hz and 1 KHz at $E = 1.82$ V (Figure 3a) and at the equilibrium potential (Figure 3b).

EIS measurements were fitted according to the model reported in Figure 3, where Rct and Cdl correspond to the charge transfer resistance of the faradaic reaction and double layer capacitance at the interface electrode/electrolyte, respectively. Under OER conditions (Figure 3a), the Rct value of 43 Ω for Au−Fe nanoalloys was remarkably lower than that of Au (268 Ω), FeO$_x$ (890 Ω) and the physical mixture of Au and FeO$_x$ (1070 Ω) NPs, which indicates that the OER kinetics is faster for Au–Fe nanoalloys, in agreement with data obtained from CV. EIS data acquired in OER conditions also show that the electrode/electrolyte interface contribution dominates over diffusion.

EIS data acquired at equilibrium potential (Figure 3b) were used to calculate the electrochemical surface area (ECSA), according to the protocol proposed by Jaramillo
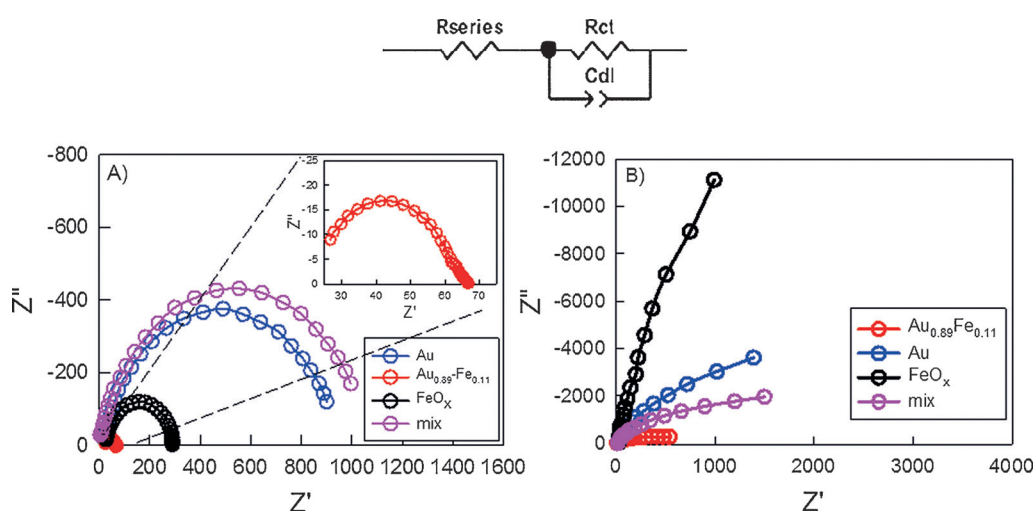

Figure 3. Nyquist plot obtained from EIS measurements performed A) under OER conditions (1.82 V vs. RHE) and B) at equilibrium potential. The model circuit utilized for fitting EIS data is shown on the top of the panel. The real and imaginary part of the impedance Z are indicated as Z′ and Z′′, respectively.

et al.[40] For the $Au_{0.89}Fe_{0.11}$ nanoalloy an ECSA of 2.14 cm^{-2} has been obtained, which is much higher in comparison to that of bare Au (ECSA = 0.76 cm^{-2}), FeO_x (ECSA = 0.31 cm^{-2}) and the physical mixture of the metals (ECSA = 0.94 cm^{-2}). The related specific current densities at $E = 1.82$ V (see Chapter S3 for calculation details) show a similar trend.

The $Au_{0.89}Fe_{0.11}$ NPs were also subjected to a stress test of 1000 CV cycles (scan rate: 300 $mV\,sec^{-1}$) to investigate their stability (see Chapter S4). Under these conditions the maximum current progressively decreases to the 37% of its initial value. These data suggest that further efforts are required prior to the integration of this type of nanoalloys in real-working devices, as shown also from the tests performed with the configuration of a whole electrochemical cell, using a Nafion thin film as a membrane (see Chapter S5).

Overall, the experimental data indicate that the Au–Fe nanoalloys result in an improved OER activity. OER mechanism is usually described to proceed from the initial adsorption of hydroxy ions that are discharged at the anode surface to form neutral OH adsorbates. Thus, depending on the type of catalyst, different steps may occur, involving the formation of a range of surface adsorbed intermediates, which concur to oxygen evolution at higher potential values.[35–37] These steps strongly depend on the chemical nature of the catalyst. For example, a recent paper demonstrated that the OER activity of Ni–Fe layered double hydroxides is directly mediated by carbonate ions, which are formed by dissolution of CO_2 in alkaline conditions and replace other interlayer anions.[37]

The analysis of Tafel plots, acquired at 0.2 $mV\,s^{-1}$ (see Chapter S6), reveals two distinct linear regions, which are commonly observed in literature. However, no specific hints on the origin of the improved OER can be inferred from Tafel analysis.[23,24]

The mutual interaction between Au and Fe (and other materials such as Co, Ni or even Mn) in OER catalysts has been the object of recent studies and is intensively investigated.[30,31] Boettcher and co-workers reported that the OER activity of FeOOH films is strongly enhanced when they are deposited on Au electrodes.[14] That study demonstrated that FeOOH is activated upon oxidation of Au to AuO_x, which leads to the formation of hydrated Au–Fe mixed surface oxides. Similar results were reported by Bell and co-workers for Fe impurities deposited on oxidized Au electrodes.[31] All these studies point out the importance of mixing Au and Fe on the atomic (i.e. subnanometric) scale, where their chemical and electronic interaction is stronger. In particular, in order to improve OER activity, the conductivity of iron must be strongly enhanced, which means that the lattice surrounding the active species should be conductive. Gold is an ideal partner to develop synergistic interactions with iron. In a recent paper, Klaus et al.[15] demonstrated that Fe^{3+} species, which are in the form of FeO_2^- anions in alkaline pH, can accumulate on the surface of oxidized gold and promote oxygen evolution through the conversion into ferrate(VI) ions (FeO_4^{2-}). They also observed that the progressive removal of Fe^{3+} during the subsequent CV cycles leads to a decrease of the overall OER activity. The high reversibility of the redox state of Fe in the Au lattice of Au–Fe nanoalloys has been also demonstrated in the recent study of Martirez and Carter.[16]

On the other hand, Karthik et al.[32] demonstrated that the Fe species present in Fenton's reagent can be exploited to produce hydroxy radicals that remove low coordinated, metastable gold atoms from the surface of Au electrodes. As a result, the modified surface of the Au electrodes becomes much more efficient in promoting OER. Thus, depending on the system under analysis, the role of iron species can be different.

In this context, the production of nanoalloys that incorporate high amounts of iron can represent a real breakthrough for the development of a new class of electrocatalysts with unexplored performances, as well as to improve the current understanding about the role of transition metals in OER.[33]

These results show that alloying noble metals with transition metals is an appealing general approach to improve electrocatalytic oxygen evolution. It has been proposed that the same effect could be obtained also in other alloys of noble metals and transition metals with partially occupied d orbitals (such as Co and Ni),[34] which still deserve to be investigated.[26–29]

Conflict of interest

The authors declare no conflict of interest.

[1] M. G. Walter, E. L. Warren, J. R. McKone, S. W. Boetcher, Q. Mi, E. A. Santori, N. S. Lewis, *Chem. Rev.* **2010**, *110*, 6446–6473.

[2] R. Subbaraman, D. Tripkovic, K.-C. Chang, D. Strmcnik, A. P. Paulikas, P. Hirunsit, M. Chan, J. Greeley, V. Stamenkovic, N. M. Markovic, *Nat. Mater.* **2012**, *11*, 550–557.

[3] W. T. Hong, M. Risch, K. A. Stoerzinger, A. Grimaud, J. Suntivich, Y. Shao-Horn, *Energy Environ. Sci.* **2015**, *8*, 1404–1427.

[4] L. Wang, J. Geng, W. Wang, C. Yuan, L. Kuai, B. Geng, *Nano Res.* **2015**, *8*, 3815–3822.

[5] B. M. Hunter, J. D. Blakemore, M. Deimund, H. B. Gray, J. R. Winkler, A. M. Müller, *J. Am. Chem. Soc.* **2014**, *136*, 13118–13121.

[6] Y. Wu, M. Chen, Y. Han, H. Luo, X. Su, M.-T. Zhang, X. Lin, J. Sun, L. Wang, L. Deng, W. Zhang, R. Cao, *Angew. Chem. Int. Ed.* **2015**, *54*, 4870–4875; *Angew. Chem.* **2015**, *127*, 4952–4957.

[7] M. Chen, Y. Wu, Y. Han, X. Lin, J. Sun, W. Zhang, R. Cao, *ACS Appl. Mater. Interfaces* **2015**, *7*, 21852–21859.

[8] G. Młynarek, M. Paszkiewicz, A. Radniecka, *J. Appl. Electrochem.* **1984**, *14*, 145–149.

[9] Y. Qiu, L. Xin, W. Li, *Langmuir* **2014**, *30*, 7893–7901.

[10] M. W. Louie, A. T. Bell, *J. Am. Chem. Soc.* **2013**, *135*, 12329–12337.

[11] L. Trotochaud, S. L. Young, J. K. Ranney, S. W. Boettcher, *J. Am. Chem. Soc.* **2014**, *136*, 6744–6753.

[12] D. Friebel, M. W. Louie, M. Bajdich, K. E. Sawald, Y. Cai, A. M. Wise, M.-J. Cheng, D. Sokaras, T.-C. Weng, R. Alonso-Mori, R. C. Davis, J. R. Bargar, J. K. Nørskov, A. Nilsson, A. T. Bell, *J. Am. Chem. Soc.* **2015**, *137*, 1305–1313.

[13] M. S. Burke, M. G. Kast, L. Trotochaud, A. M. Smith, S. W. Boettcher, *J. Am. Chem. Soc.* **2015**, *137*, 3638–3648.

[14] S. Zou, M. S. Burke, M. G. Kast, J. Fan, N. Danilovic, S. W. Boettcher, *Chem. Mater.* **2015**, *27*, 8011–8020.

[15] S. Klaus, L. Trotochaud, M.-J. Cheng, M. Head-Gordon, A. T. Bell, *ChemElectroChem* **2016**, *3*, 66–73.

[16] J. M. P. Martirez, E. A. Carter, *ACS Nano* **2016**, *10*, 2940–2949.

[17] H. Okamoto, *Desk Handbook: Phase Diagrams for Binary Alloys*, ASM International, Ohio, **2000**.

[18] V. Amendola, S. Scaramuzza, S. Agnoli, S. Polizzi, M. Meneghetti, *Nanoscale* **2014**, *6*, 1423–1433.

[19] J. Zhang, M. Chaker, D. Ma, *J. Colloid Interface Sci.* **2017**, *489*, 138–149.

[20] J. Zhang, G. Chen, D. Guay, M. Chaker, D. Ma, *Nanoscale* **2014**, *6*, 2125–2130.

[21] S. Gu, J. Kaiser, G. Marzun, A. Ott, Y. Lu, M. Ballauff, A. Zaccone, S. Barcikowski, P. Wagener, *Catal. Lett.* **2015**, *145*, 1105–1112.

[22] J. D. Blakemore, H. B. Gray, J. R. Winkler, A. M. Müller, *ACS Catal.* **2013**, *3*, 2497–2500.

[23] M. E. G. Lyons, R. L. Doyle, M. P. Brandon, *Phys. Chem. Chem. Phys.* **2011**, *13*, 21530–21551.

[24] M. E. G. Lyons, R. L. Doyle, *Int. J. Electrochem. Sci.* **2012**, *7*, 9488–9501.

[25] E. Pizzolato, S. Scaramuzza, F. Carraro, A. Sartori, S. Agnoli, V. Amendola, M. Bonchio, A. Sartorel, *J. Energy Chem.* **2016**, *25*, 246–250.

[26] B. S. Yeo, A. T. Bell, *J. Am. Chem. Soc.* **2011**, *133*, 5587–5593.

[27] Y.-H. Fang, Z.-P. Liu, *ACS Catal.* **2014**, *4*, 4364.

[28] T. Shinagawa, A. T. Garcia-Esparza, K. Takanabe, *Sci. Rep.* **2015**, *5*, 13801.

[29] Y. Gorlin, C.-J. Chung, J. D. Benck, D. Nordlund, L. Seitz, T.-C. Weng, D. Sokaras, B. M. Clemens, T. F. Jaramillo, *J. Am. Chem. Soc.* **2014**, *136*, 4920–4926.

[30] R. Frydendal, M. Busch, N. B. Halck, E. A. Paoli, P. Krtil, I. Chorkendorff, J. Rossmeisl, *ChemCatChem* **2015**, *7*, 149–154.

[31] B. S. Yeo, S. L. Klaus, P. N. Ross, R. A. Mathies, A. T. Bell, *ChemPhysChem* **2010**, *11*, 1854.

[32] P. E. Karthik, C. Jeyabharathi, K. L. Phani, *Chem. Commun.* **2014**, *50*, 2787.

[33] Z. Xu, Y. Liu, F. Ren, F. Yang, D. Ma, *Coord. Chem. Rev.* **2016**, *320–321*, 153–180.

[34] A. Holewinski, J.-C. Idrobo, S. Linic, *Nat. Chem.* **2014**, *6*, 828–834.

[35] B. M. Hunter, H. B. Gray, A. M. Müller, *Chem. Rev.* **2016**, *116*, 14120–14136.

[36] D. A. Corrigan, *J. Electrochem. Soc.* **1987**, *134*, 377–384.

[37] B. M. Hunter, W. Hieringer, J. R. Winkler, H. B. Gray, A. M. Müller, *Energy Environ. Sci.* **2016**, *9*, 1734–1743.

[38] F.-J. Lai, H.-L. Chou, L. S. Sarma, D.-Y. Wang, Y.-C. Lin, J.-F. Lee, B.-J. Hwang, C.-C. Chen, *Nanoscale* **2010**, *2*, 573–581.

[39] S. Kawata, K. Maeda, *J. Phys. C* **1978**, *11*, 2391–2397.

[40] C. C. L. McCRory, S. Jung, J. C. Peters, T. F. Jaramillo, *J. Am. Chem. Soc.* **2013**, *135*, 16977–16987.

[41] S. Jung, C. C. L. McCrory, I. M. Ferrer, J. C. Peters, T. F. Jaramillo, *J. Mater. Chem. A* **2016**, *4*, 3068–3076.